ELSEVIER

Journal of Alloys and Compounds 408–412 (2006) 780–783

Journal of ALLOYS AND COMPOUNDS

www.elsevier.com/locate/jallcom

Spectroscopic properties of Yb doped YLF grown by a vertical Bridgman method

Akira Sugiyama [a,*], Masamichi Katsurayama [b], Yutaka Anzai [b], Taiju Tsuboi [c]

[a] *Japan Atomic Energy Research Institute, Kizu, Souraku-gun, Kyoto 619-0215, Japan*
[b] *Mitsui Mining and Smelting Co., Ltd., Haraichi, Ageo-shi, Saitama 362-0021, Japan*
[c] *Kyoto Sangyo University, Kamigamo, Kita-ku, Kyoto 603-8555, Japan*

Received 31 July 2004; received in revised form 9 December 2004; accepted 13 January 2005
Available online 8 June 2005

Abstract

Laser crystals of $LiYF_4$ (YLF) doped with 5–64 at.% of trivalent ytterbium ions (Yb^{3+}) were grown by a vertical Bridgman method. As crystal growth materials of YbF_3 and YF_3 including YOF impurities caused opaque crystal, the YOF reduction procedure using PbF_2 was essential before starting the crystal growth. We derived seven energy levels from the $^2F_{7/2}$ and $^2F_{5/2}$ manifolds of Yb^{3+}:YLF by the crystal-field analysis from which we explain the observed polarized absorption and emission spectra. The intrinsic broad and complicated spectra of Yb^{3+}:YLF are attributed to the strong coupling of the 4f electrons with lattice vibration of the crystal.

Keywords: Yb; YLF; Laser crystal; Crystal growth; Bridgman method; Spectroscopy; Energy levels; Crystal-field parameters

1. Introduction

Laser crystals doped with Yb^{3+} ions including Yb^{3+} doped $LiYF_4$ (YLF) [1,2] are of interest for the development of advanced high-peak power lasers [3,4]. As Yb^{3+} ions with thirteen 4f-electrons have two simple manifolds of the $^2F_{5/2}$ excitation state and the $^2F_{7/2}$ ground state, the Yb^{3+} lasers possess several advantages, for examples, no energy loss caused by excited state absorption (ESA), high quantum efficiency, and large accumulation power of optical energy derived from long (ms order) decay of the upper states. However, the 4f-electron which is shielded by s^2p^6 closed shell in rare earth elements usually does not have a strong interaction with the surrounded crystal field, which results in narrower line width of absorption and emission spectra in comparison of laser crystals doped with transition metal ions of Cr^{3+} and Ti^{3+} which are used in ultra short pulse lasers. Furthermore, hard optical pumping for the laser oscillation increases population densities at the upper Stark sub-manifolds in the $^2F_{7/2}$ ground state, which tends to drop the laser output power. To overcome these disadvantages, Yb^{3+}:YLF cooled by liquid N_2 has been investigated for the development of the chirped pulse amplification (CPA) laser that can generate sub-pico second laser pulses [5].

As Yb^{3+}:YLF crystal has broad emission spectrum and negative refractive index change with increasing temperature, the crystal is one of the promising candidates for the CPA laser. In usual case, YLF laser crystals doped with rare earth ions have been grown by the Czochralski method that requires continuous supply of hazardous HF or CF_4 gas. Compared with this method, the simple Bridgman method might have economical benefit in case of the crystal enlargement. In addition, in spite of distinct information of the Stark sub-manifolds energy levels is essential for the laser crystal evaluation, various data of Yb^{3+}:YLF have been reported [1,2,6,7]. From these viewpoints, we have tried to grow Yb^{3+}:YLF by the Bridgman method and have studied its spectroscopic properties.

* Corresponding author. Tel.: +81 774 71 3365; fax: +81 774 71 3316.
E-mail address: sugiyama@apr.jaeri.go.jp (A. Sugiyama).

0925-8388/$ – see front matter © 2005 Published by Elsevier B.V.
doi:10.1016/j.jallcom.2005.01.094

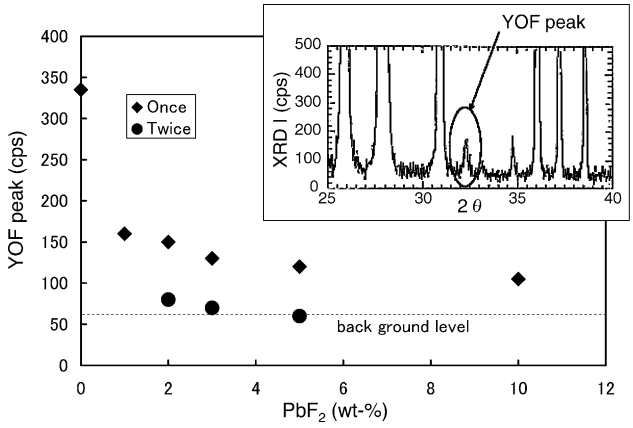

Fig. 1. YOF Reduction by the material treatment with PbF_2 scavenger. Once and twice mean the number of reduction process. The inset shows the YOF peak measured in XRD analysis after the treatment.

2. Experimental procedure

Yb^{3+}:YLF crystals were grown by our original built of two-zone resistance heating furnace using the Bridgman–Stockbarger technique. From previous works, we improved the temperature gradient by adjusting heater currents and modified insulator configuration surrounding the crucible to realize the suitable temperature condition of 30–40 K/cm. The reduction process of YOF impurity was essential for the starting materials of YF_3 and YbF_3 powder prior to the YLF crystal growth. PbF_2 powders were mixed to remove the unintentionally contained YOF impurity by the chemical reaction of $YOF + PbF_2 \rightarrow YF_3 + PbO$, where the produced PbO evaporates during the heat treatment at 1430 K in a vacuum furnace for 5 h. From evaluations of powder X-ray diffraction (XRD) analysis, we recognized that twice of the process can reduce YOF impurity down to negligible small, as shown in Fig. 1.

The incongruent melt of YLF crystal has the peritectic point at 1092 K in 49 mol.% of YF_3, and LiF is easy to evaporate above the melting point. Several Li-rich melt composition of $LiF:(YF_3 + YbF_3) = 51:49–60:40$ in mol.% were tested in the crystal growth. The higher Li-rich composition showed enhancement of transparent area inside the crystal boules. From the result, we fixed the composition of 60:40, and tried YLF crystals growth doped with Yb^{3+} of 5, 10, 20, 40 and 60 at.%. The mixed charge was placed in a graphite crucible with a diameter of 34 mm. Then, it was evacuated in the furnace down to 10^{-4} Pa so as to be free of oxygen. The crystals were lowered at a rate of 1 mm/h. After translating of 12 cm, the crystals were cooled over a period of 24 h. The as-grown crystal boules were 11 cm total length, and about a half length had transparent crystal. We extracted specimens from each boule and measured the lattice constants by the XRD analyzer, the amount of Yb ions by inductively coupled plasma atomic emission spectroscopy (ICP-AES), and other properties. These data are summarized in Table 1.

The optical absorption spectra and emission spectra were measured by a spectrometer in the temperature range of 15–300 K. Before the measurements, Yb^{3+}:YLF samples were polished to a thickness less than 1 mm and mounted in a copper block installed in a cryogenic refrigerator. In the emission measurements, the excitation beam from a polarized laser diode was focused into the sample. In the absorption measurements, the probe beam emitted from a xenon lamp was filtered by a monochromator. To discriminate against the pump or probe light, an optical chopper was inserted for each beam and the detected signal was captured on a lock-in amplifier triggered by the chopper. In the optical measurements, the spectral resolution was less than about 10 cm^{-1} in wave number.

3. Experimental results and discussion

Fig. 2 shows the polarized absorption and emission spectra measured in our spectrometer. At 300 K, the spectra are extremely broad and the intensities are small. Some spectral structure can be seen as the temperature decreases, however, we cannot find the distinctive structure corresponding to each transition between two manifold levels even at the lowest temperature of 15 K. On the other hand, it was reported that $CaWO_4$ host crystal with the same scheelite as YLF shows three well separated groups including clear zero phonon line in the absorption spectrum [8]. Yb ions would have strong interaction with the surrounding YLF crystal lattice.

Fig. 3 shows the absorption spectra in two different polarizations. The zero phonon level corresponding to the transition of E1–E5 is found in the 10,288 cm^{-1}. As the site of Yb^{3+} in YLF is S_4 symmetry, degenerated Kramer's doublets written in the irreducible representations are assigned to each Stark splitting level [8]. According to the selection rules for the transition of E1–E7, σ-polarized transition is

Table 1
Measured properties of grown Yb^{3+}:YLF crystals

Specimens	Yb constant (at.%)	Density (g/cm^3)	Yb ions (cm^{-3})	Lattice constant (Å)	
				a	*c*
$LiYb_{0.05}Y_{0.95}F_4$	4.45	4.08	6.21×10^{20}	5.1691	10.7300
$LiYb_{0.1}Y_{0.9}F_4$	9.23	4.18	1.29×10^{20}	5.1670	10.7226
$LiYb_{0.2}Y_{0.8}F_4$	20.67	4.32	2.90×10^{21}	5.1623	10.7028
$LiYb_{0.4}Y_{0.6}F_4$	41.02	4.61	5.78×10^{21}	5.1560	10.6718
$LiYb_{0.6}Y_{0.4}F_4$	63.88	5.14	9.06×10^{21}	5.1495	10.6419

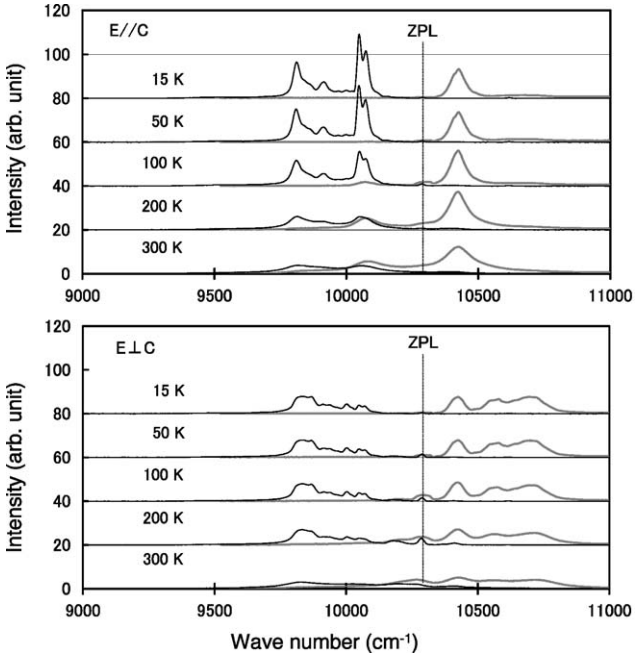

Fig. 2. Polarized spectra of 64 at.% Yb^{3+} doped YLF at various temperature between 15 K and 300 K. Black and gray lines show the emission and absorption spectra, respectively. ZPL means the zero phonon line.

allowed by electric and magnetic dipoles, on the other hand, π-polarized transition is only allowed by magnetic-dipole. Since the electric-dipole transition probability is quite larger than the magnetic-dipole transition probability, it is concluded that the large signal measured in σ-polarization of around 10,600 cm^{-1} corresponds to the transition of E1–E7.

We consider crystal-field energy levels of Yb^{3+}:YLF. The Hamiltonian for S_4 symmetry is given by:

$$H_{CF} = B_0^2 C_0^{(2)} + B_0^4 C_0^{(4)} + B_0^6 C_0^{(6)} + B_4^4 C_4^{(4)} + (B_4^6 + B_4'^6) C_4^6$$

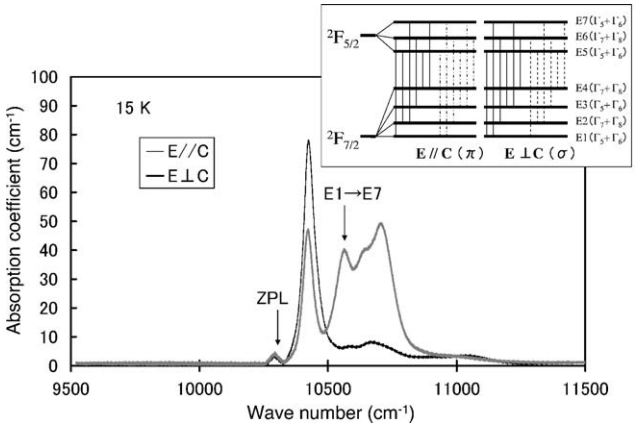

Fig. 3. The polarized absorption spectra measured at 15 K. ZPL means zero phonon level. The inset shows available transitions derived from the selection rules in each polarization [9]; broken line means electric-dipole transition, one point broken line means magnetic-dipole transition and solid line means both dipole transitions, respectively.

where all symbols are defined in Ref. [10]. To obtain the crystal-field splitting of $^2F_{7/2}$ and $^2F_{5/2}$ states, we used the results of reduced matrix elements [11] and 3-j and 6-j symbols [12]. For the derivation, we referred to Ref. [13]. Each level is written by the matrix elements as follows. In the $^2F_{7/2}$ state:

$$E1,\ E3 = \frac{b_{11} + b_{22} \pm \sqrt{(b_{11} - b_{22})^2 + 4{b_{12}}^2}}{2} \quad \text{and}$$

$$E2,\ E4 = \frac{a_{11} + a_{22} \pm \sqrt{(a_{11} - a_{22})^2 + 4{a_{12}}^2}}{2}$$

$$a_{11} = \left\langle \frac{7}{2}\frac{1}{2} \middle| H_{CF} \middle| \frac{7}{2}\frac{1}{2} \right\rangle, \quad a_{22} = \left\langle \frac{7}{2} - \frac{7}{2} \middle| H_{CF} \middle| \frac{7}{2} - \frac{7}{2} \right\rangle,$$

$$a_{12} = \left\langle \frac{7}{2} - \frac{7}{2} \middle| H_{CF} \middle| \frac{7}{2}\frac{1}{2} \right\rangle$$

$$b_{11} = \left\langle \frac{7}{2}\frac{5}{2} \middle| H_{CF} \middle| \frac{7}{2}\frac{5}{2} \right\rangle, \quad b_{22} = \left\langle \frac{7}{2} - \frac{3}{2} \middle| H_{CF} \middle| \frac{7}{2} - \frac{3}{2} \right\rangle,$$

$$b_{12} = \left\langle \frac{7}{2} - \frac{3}{2} \middle| H_{CF} \middle| \frac{7}{2}\frac{5}{2} \right\rangle$$

and in the $^2F_{5/2}$ state,

$$E5,\ E7 = \frac{b_{33} + b_{44} \mp \sqrt{(b_{33} - b_{44})^2 + 4{b_{34}}^2}}{2} \quad \text{and}$$

$$E6 = \left\langle \frac{5}{2}\frac{1}{2} \middle| H_{CF} \middle| \frac{5}{2}\frac{1}{2} \right\rangle = -\frac{2}{105}[12B_0^2 + 5B_0^4]$$

$$b_{33} = \left\langle \frac{5}{2}\frac{5}{2} \middle| H_{CF} \middle| \frac{5}{2}\frac{5}{2} \right\rangle, \quad b_{44} = \left\langle \frac{5}{2} - \frac{3}{2} \middle| H_{CF} \middle| \frac{5}{2} - \frac{3}{2} \right\rangle,$$

$$b_{34} = \left\langle \frac{5}{2} - \frac{3}{2} \middle| H_{CF} \middle| \frac{5}{2}\frac{5}{2} \right\rangle$$

Table 2 presents the calculated crystal-field parameters by the point charge model, together with the results by Brown [16]. One large discrepancy is found in the $B_4'^6$ imaginary parameter. We cannot explain the reason of difference, and further improvement of the model would be required. Table 2 also summarizes the energy levels calculated with our optimized parameters and energy levels assigned by various scientists.

The experimental data well support to the results reported by Refs. [1,2]. In the comparison of our results and Refs. [6,7], the discrepancy is found in the E7 level. Fig. 4 shows computer deconvolution of the assigned transition levels and vibronic transitions based on Raman active spectra measured in YLF crystal [14,15]. Since the phonons couple with different electronic levels, the corresponding vibronic spectra appear in the absorption spectrum, giving rise to the complicated and broad spectra. The 10,730 cm^{-1} line in Ref. [7] is suggested to arise from coupling with the vibration mode of crystal lattice (see Fig. 4).

Table 2
The fitted crystal-field parameters and the comparison of assigned energy levels of the ^2L_J manifold. Concerning the energy difference between E1 and E5, we assigned 10,288 cm^{-1} which was measured in Fig. 3. The calculated and measured energy levels were assigned with the accuracy of $\pm 10\ cm^{-1}$

Crystal-field parameters (cm^{-1})						References
B_0^2	B_0^4	B_0^6	B_4^4	B_4^6	B'^6_4	
285	−560	−10	530	350	960	This work
284	−432	−11	585	283	35	[16]

$^2F_{7/2}$ (cm^{-1})				$^2F_{5/2}$ (cm^{-1})			References
E1	E2	E3	E4	E5	E6	E7	
0	236	398	449	10288	10409	10566	Calculated
0	237	375	477	10288	10420	10570	Experimental
0	216	371	479	10288	10409	10547	[1]
0	212	364	455	10259	10399	10533	[2]
0	235	366	456	10259	10404	10628	[6]
0	224	359	438	10270	10400	10730	[7]

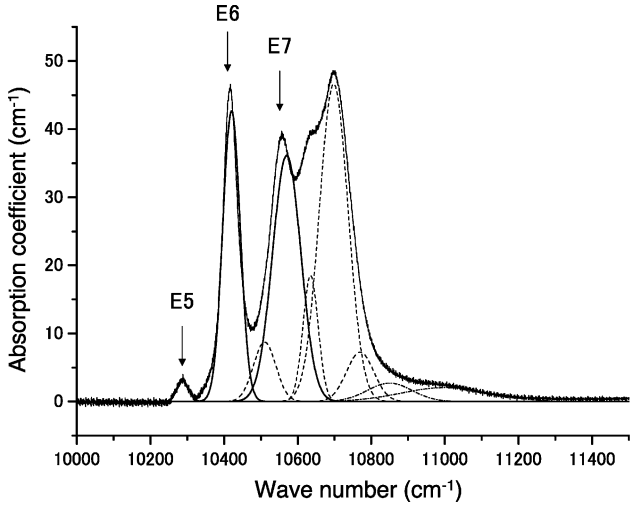

Fig. 4. Fitting model of the absorption spectra, including coupling with vibration components of the crystal lattice. The transitions from the ground state of E1–E5, E6 and E7 are indicated by arrows. The broken and one point broken lines mean the vibronic replicas of E5 and E7 transitions, respectively.

4. Conclusions

We have succeeded in the YLF crystal growth doped with Yb^{3+} ions of 5–64 at.% by the simplified Bridgman method. Purification of YF_3 and YbF_3 was essential to grow transparent fluoride YLF crystals. Optical absorption and emission spectra were measured at 15–300 K. We performed the crystal-field analysis based on the S_4 symmetry of Yb^{3+} in YLF to explain the observed emission and absorption spectra, and we derived seven Stark splitting energy levels. Our results were consistent with the result by Brown et al. We have also explained the complicated and broad absorption spectrum of Yb^{3+}:YLF by means of the deconvolution of the electric transition and vibronic mode.

References

[1] E.A. Brown, Harry Diamond Laboratories Reports TR-1932, NTIS #091252, 1980.
[2] J.E. Miller, E.J. Sharp, J. Appl. Phys. 41 (1970) 4718.
[3] L.D. DeLoach, S.A. Payne, L.L. Chase, l.K. Smith, W.L. Kway, W.F. Krupke, IEEE J. Quantum Electron. 29 (1993) 1179.
[4] C. Stewen, M. Larionov, A. Giesen, k. Contag, OSA TOPS 34 (2000) 35.
[5] J. Kawanaka, H. Nishioka, N. Inoue, K. Ueda, Appl. Opt. 40 (2001) 3542.
[6] A.K. Kupchikov, B.Z. Malkin, A.L. Natadze, A.I. Ryskin, Sov. Phys. Solid State 29 (1987) 1913.
[7] N. Uehara, K. Ueda, Y. Kubota, Jpn. J. Appl. Phys. 35 (1996) L499.
[8] G.R. Jones, J. Chem. Phys. 47 (1967) 4347.
[9] N. Karayianis, R.T. Farrar, J. Chem. Phys. 53 (1970) 3436.
[10] B.G. Wybourne, Spectroscopic Properties of Rare Earths, Interscience Publisher, NY, 1965.
[11] C.W. Nielson, G.F. Koster, Spectroscopic Coefficients for the p^n, d^n and f^n Configurations, M.I.T., Cambridge, MA, 1963.
[12] M. Rotenberg, R. Bivins, N. Metropolis, J.K. Wooten Jr., The 3-j and 6-j Symbols, M.I.T., Cambridge, MA, 1959.
[13] C.A. Morrison, Angular Momentum Theory Applied to Interactions in Solids, Springer-Verlag, NY, 1988.
[14] S.A. Miller, H.E. Rast, H.H. Caspers, J. Chem. Phys. 52 (1970) 4172.
[15] S. Salaun, M.T. Fornoni, A. Bulou, M. Rousseau, P. Simon, J.Y. Gesland, J. Phys. Condens. Matter 9 (1997) 6941.
[16] E.A. Brown, Harry Diamond Laboratories Reports TR-1934, NTIS #0900976, 1980.